Multiplexing molecular tension sensors reveals piconewton force gradient across talin-1

Pia Ringer[1], Andreas Weißl[2], Anna-Lena Cost[1], Andrea Freikamp[1], Benedikt Sabass[3], Alexander Mehlich[2], Marc Tramier[4–6], Matthias Rief[2,7] & Carsten Grashoff[1]

© 2017 Nature America, Inc., part of Springer Nature. All rights reserved.

Förster resonance energy transfer (FRET)-based tension sensor modules (TSMs) are available for investigating how distinct proteins bear mechanical forces in cells. Yet, forces in the single piconewton (pN) regime remain difficult to resolve, and tools for multiplexed tension sensing are lacking. Here, we report the generation and calibration of a genetically encoded, FRET-based biosensor called FL-TSM, which is characterized by a near-digital force response and increased sensitivity at 3–5 pN. In addition, we present a method allowing the simultaneous evaluation of coexpressed tension sensor constructs using two-color fluorescence lifetime microscopy. Finally, we introduce a procedure to calculate the fraction of mechanically engaged molecules within cells. Application of these techniques to new talin biosensors reveals an intramolecular tension gradient across talin-1 that is established upon integrin-mediated cell adhesion. The tension gradient is actomyosin- and vinculin-dependent and sensitive to the rigidity of the extracellular environment.

Mechanical forces of just a few pN can regulate the activity of proteins and thereby modulate a wide range of biological processes[1,2]. Forces of about 3–5 pN, for instance, speed proteolytic cleavage of the Notch receptor[3], while the affinity of the actin crosslinking protein filamin to its binding partners increases after application of 2–5 pN[4]. Binding of the cell adhesion protein vinculin to the integrin activator talin-1 is induced by mechanical tension of 2–12 pN[5], and the cadherin–catenin interaction, which is central to intercellular cohesion, strengthens under mechanical loads of about 5 pN[6]. *In vitro*, cytoskeletal motor proteins like myosins generate exactly these magnitudes of force—namely, about 4–5 pN per motor protein[7]. FRET-based tension sensors have been developed to quantify such pN-scale forces, and different molecular designs have been realized to determine forces within cells[8,9] or at the cell surface[10–12].

Genetically encoded probes are ideally suited to measure intracellular forces. They typically comprise two GFP-like fluorophores connected by a mechanosensitive linker peptide that extends in response to mechanical tension[13]. As FRET is distance dependent, forces elongating the linker peptide reduce FRET, which can be quantified microscopically. Our first single-molecule-calibrated TSM used the 40 amino acid (aa)-long flagelliform peptide (F40), which behaves like a molecular spring and gradually elongates when forces between 1–6 pN[8] are applied. To quantify greater forces, we developed a biosensor using the 35-aa-long villin headpiece peptide (HP), which responds to about 6–8 pN[9]; a third biosensor was based upon a stabilized HP peptide (HPst) that displayed maximal sensitivity at 9–11 pN[9]. These TSMs have been applied to study various mechanotransduction processes in cells; notably, the F40-TSM has been extensively used in a range of cell types and model organisms[13–18]. Owing to the gradual FRET response of the F40 module, however, forces below 6 pN have remained difficult to resolve[13,19], and it has been virtually impossible to determine how many molecules of a given population are mechanically engaged. Moreover, methods to analyze distinct force sensor constructs within the same cell have been lacking. We addressed these limitations by developing a novel 3–5-pN-sensitive TSM, establishing a method to evaluate two coexpressed TSMs simultaneously, and introducing a data analysis algorithm to estimate the fraction of mechanically engaged sensor molecules.

RESULTS

Generation and calibration of a 3–5-pN-sensitive tension sensor module

Live-cell tension sensor experiments are typically performed as ensemble measurements that provide an average force value. When TSMs with a spring-like force response are used, it is challenging to determine how much tension individual molecules experience in cells, as the percentage of molecules actively engaged in a given force transduction process is usually unknown[13,19]. To address this problem, we engineered a new TSM through using a ferredoxin-like (FL) linker peptide that was expected to display more digital force response characteristics (**Fig. 1a**)[20]. Indeed,

[1]Group of Molecular Mechanotransduction, Max Planck Institute of Biochemistry, Martinsried, Germany. [2]Physics Department E22, Technical University of Munich, Garching, Germany. [3]ICS-2/IAS-2, Forschungszentrum Jülich, Jülich, Germany. [4]CNRS, UMR 6290, Rennes, France. [5]Institut de Génétique et Développement de Rennes, Université de Rennes, Rennes, France. [6]Microscopy Rennes Imaging Centre, Université de Rennes, Rennes, France. [7]Munich Centre for Integrated Protein Science, Munich, Germany. Correspondence should be addressed to C.G. (cgrasho@biochem.mpg.de).

RECEIVED 12 APRIL; ACCEPTED 18 AUGUST; PUBLISHED ONLINE 18 SEPTEMBER 2017; DOI:10.1038/NMETH.4431

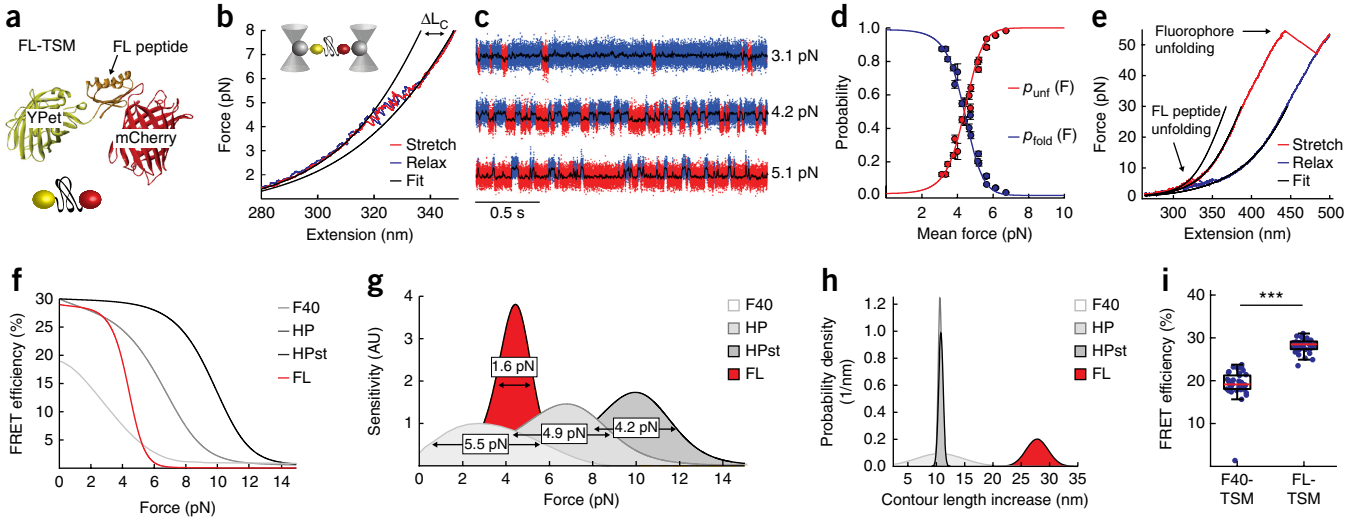

Figure 1 | Calibration of FL-TSM. (**a**) Schematic of FL-TSM. (**b**) Representative example of stretch–relax trace fitted with an extensible worm-like chain model (black line); the overlapping stretch (red) and relax (blue) traces indicate the absence of hysteresis (pulling velocity 10 nm/s). ΔL_C indicates the observed contour length increase. (**c**) Representative passive mode traces at 3.1 pN, 4.2 pN, and 5.1 pN. Folded FL states are colored in blue and unfolded FL states are in red. (**d**) Probability of FL-TSM to be in the folded (blue) or unfolded (red) state at a given force. (**e**) Representative stretch–relax trace covering 1–55 pN (pulling velocity 100 nm/s). Note that fluorophores unfold at much higher forces as compared to the FL peptide. (**f**) FRET–force correlation of FL-TSM (red) compared with previously described TSMs (gray). FL-TSM (red) is characterized by a sharp transition between 3–5 pN. (**g**) Sensitivity–force correlation of single-molecule-calibrated TSMs. FL-TSM (red) displays the sharpest force response as indicated by the full width at half maximum values. (**h**) Histograms of experimentally observed contour length increases ΔL_C. FL-TSM (red) yields an average maximum extension of 27.4 ± 2.8 nm (n = 269 unfolding events from 15 FL-TSM molecules in six independent experiments), while the previously described TSMs (grays) yield a mean contour length gain of about 11 nm. (**i**) Live-cell FLIM analysis of F40-TSM and FL-TSM expressed in the cytoplasm of cells (n = 38 and 33 cells, pooled from three independent experiments; Kolmogorov–Smirnov (KS) test; ***, $P < 0.001$). See Online Methods for definition of box plot elements.

calibration of the purified FL-TSM by single-molecule force spectroscopy revealed that the FL peptide remains in the folded state up to about 3 pN, whereas increasing tension to 5 pN induces a fast transition to the open state; both states were equally populated at about 4 pN. Unfolding was reversible, and FL sensors quickly returned to their original conformation once the mechanical load was reduced to below 3 pN. Furthermore, fluorophores remained stably folded until forces of about 40–55 pN were applied (**Fig. 1b–e**), as has been previously described[9,21].

To allow a direct comparison with F40-TSM, which was originally calibrated in the absence of fluorophores attached to N and C terminals and with a different instrument[8], we purified the full-length F40-TSM and reanalyzed F40-TSM molecules with the dual-trap optical tweezer setup. Consistent with previously published results[8], we did not observe a characteristic unfolding event as shown for the FL-TSM. Instead, the data suggested a gradual extension of the F40 peptide at low-pN force (**Supplementary Fig. 1**). Together, these experiments demonstrate that FL-TSM and F40-TSM display very different force responses.

Converting the force–extension data into FRET–force and sensitivity–force correlations confirmed the unique properties of FL-TSM (see Online Methods and **Supplementary Fig. 2**). The new probe displayed the highest sensitivity of all single-molecule-calibrated, genetically encoded TSMs reported thus far (**Fig. 1f, g**); the force-induced contour length increase was significantly larger for the FL linker than for previously developed sensor peptides, and FL-TSM displayed higher zero-force FRET efficiencies than the F40-based module, which indicated efficient peptide folding in cells (**Fig. 1h,i**). Hence, the novel biosensor should allow more accurate intracellular force measurements in the low-pN force regime.

Generation of new talin biosensors to evaluate tension across the talin rod domain

To test the performance of FL-TSM in living cells, we applied it to talin-1. Talin-1 is an essential cell adhesion protein comprising an N-terminal head domain that binds and activates integrin receptors; the C-terminal talin rod domain is made of thirteen helical bundles, which connect to the actomyosin cytoskeleton by two f-actin binding sites (called ABS2 and ABS3) as well as 11 vinculin binding motifs[22,23]. We had previously inserted the HP-TSM between the talin head and talin rod domains at aa 447 (a construct hereafter called talin-HP-447) and demonstrated that talin molecules experience forces of more than 7 pN during cell adhesion[9]. Yet it remained unclear how tension is distributed across the 190-kDa-long talin rod domain.

Therefore, we generated a set of talin biosensors in which HP- or FL-TSM was inserted at two distinct sites of the talin rod domain—namely, at aa 447 and between the two actin-binding sites at aa 1973. As controls, we fused talin-1 C terminally with the donor fluorophore YPet or either the HP- or FL-TSM, or we internally tagged talin-1 with individual fluorophores (**Fig. 2a** and **Supplementary Fig. 3**). Expression of either of these constructs rescued the adhesion and spreading phenotype of fibroblasts lacking talin-1 and talin-2 ($Tln1^{-/-}Tln2^{-/-}$); and the size of focal adhesions (FAs) was equally restored (**Fig. 2b,c** and **Supplementary Fig. 4**). The subcellular dynamics of talin were similar to those described in previously published results[9]; and internally or C terminally tagged constructs displayed comparable FA turnover rates as determined by fluorescence recovery after photobleaching (FRAP) experiments (**Fig. 2d,e**). Moreover, the fluorescence lifetimes of the integrated fluorophores were unchanged at positions aa 447 and aa 1973 (**Fig. 2f**), and intermolecular FRET at

© 2017 Nature America, Inc., part of Springer Nature. All rights reserved.

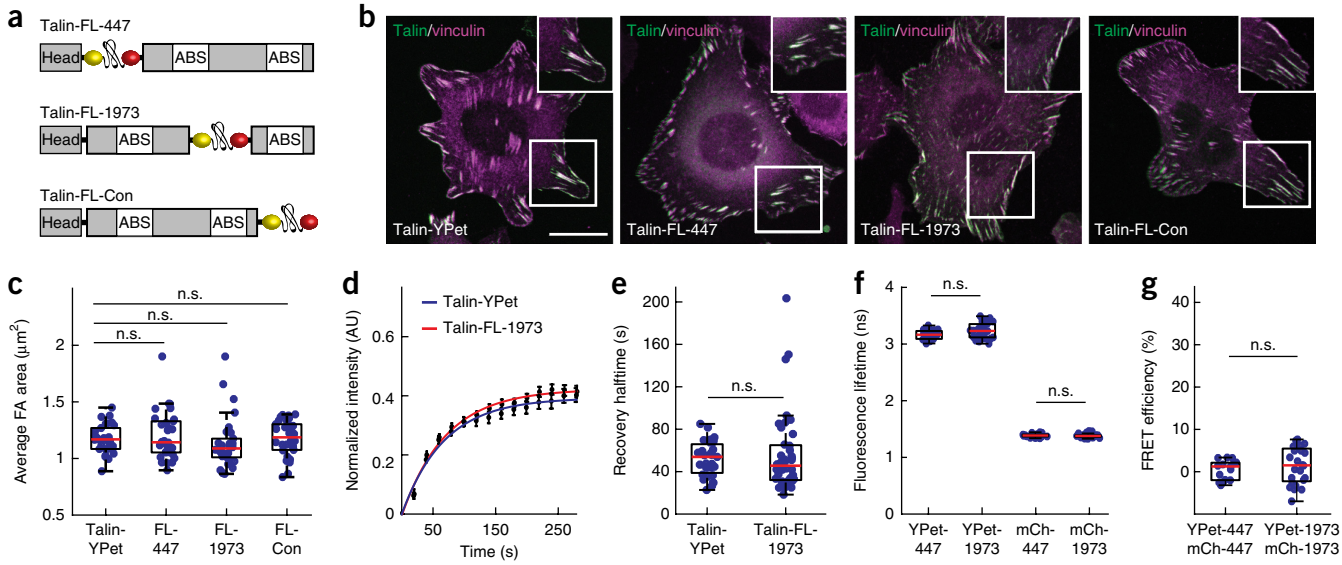

Figure 2 | Evaluation of FL-TSM-based talin tension sensors. (**a**) Schematic illustration of FL-based talin tension sensor constructs. FL-TSM was inserted after aa 447 or after aa 1973; as a control, the FL-TSM was C terminally fused to talin-1. (**b**) Stable expression of talin constructs (green) in Tln1$^{-/-}$Tln2$^{-/-}$ cells reveals normal subcellular localization to FAs marked by vinculin (magenta); scale bar, 20 µm. (**c**) FA analysis reveals comparable average FA sizes in control and tension-sensor-expressing cells (n = 30, 30, 30, 30 cells, pooled from three independent experiments). (**d**) FRAP experiments in cells expressing talin-YPet (blue) or talin-FL-1973 (red) showing normal talin-1 turnover dynamics in FAs (error bars indicate s.e.m; n = 31 and 40 cells, pooled from six independent experiments). (**e**) Normal fluorescence recovery halftimes in talin-FL-1973 cells as compared to those in talin-YPet expressing cells. (**f**) The fluorescence lifetimes of YPet and mCherry are unaffected by integration into talin-1 at aa 447 or aa 1973 (n = 22, 28, 23, 34 cells, pooled from five independent experiments). (**g**) Intermolecular FRET at position aa 447 and aa 1973 is similarly low (n = 15, 24 cells, pooled from four independent experiments). (**c**,**e**–**g**, KS test; n.s., not significant, $P > 0.05$).

aa 1973 was similarly low as for aa 447 (**Fig. 2g**). Together, these results show that TSMs can be inserted into talin-1 at aa 447 and at aa 1973 without disturbing talin function or the fluorophore's photophysical properties.

Talin-1 displays an intramolecular tension gradient during cell adhesion

To determine FRET efficiencies in living cells, we performed fluorescence lifetime imaging microscopy (FLIM) experiments as previously described[9,24] and as illustrated in **Supplementary Figure 5**. Consistent with previous measurements[9], evaluation of the HP-based talin sensor indicated an average mechanical tension of more than 7 pN at aa 447 when cells were seeded on fibronectin (FN)-coated glass slides. As a control, cells were analyzed on poly-L-Lysine (pLL)-coated surfaces, upon which FAs do not form. Remarkably, FRET efficiencies in cells expressing talin-HP-1973 were indistinguishable from pLL control values, and this suggested that the C-terminal part of the talin rod domain does not experience forces higher than 7 pN (**Fig. 3a**). Results of the respective FL-based talin sensors were consistent with high tension at aa 447; however, FRET efficiency values for cells expressing talin-FL-1973 were lower than control levels, which indicated mechanical tension of more than 3 pN at aa 1973 (**Fig. 3b**).

Since F40-TSM should also respond to the low forces observed at aa 1973 (**Fig. 1f,g**), we generated a set of F40-based talin sensors to confirm our observations. Indeed, F40-based measurements yielded similar results, but differences of talin-F40-1973 to control conditions were significantly smaller (**Fig. 3c**). As fluorescence intensities were comparable between all constructs and did not correlate with fluorescence lifetime values (**Supplementary Fig. 6**), the less pronounced differences in F40-based measurements are likely a result of the limited dynamic range of F40-TSM. More importantly, the data did not allow us to estimate how much tension individual talin molecules experience at aa 1973, owing to the gradual force–FRET response characteristics of F40-TSM (**Fig. 1f,g** and **Supplementary Fig. 1**)[8]. By contrast, FL-TSM-based measurements indicated that forces must have surpassed 3 pN to cause a significant decrease in FRET efficiencies (**Fig. 1c–g**).

To validate the FL-TSM-based measurements with an independent FRET method, we performed ratiometric imaging. Consistent with the experiments described above, we observed low FRET indices for cells expressing talin-FL-447 and increased FRET values at aa 1973; again, FRET in cells expressing talin-FL-1973 was lower than control levels (**Fig. 3d,e**).

Together, the data suggested that the talin rod domain experiences a force gradient upon integrin-mediated cell adhesion. These forces exceed 7 pN between talin head and talin rod domains, and they exceed 3 pN between the C-terminal ABSs.

Forces at talin's C-terminal region are sensitive to myosin activity and focal adhesion morphology

Next, we treated talin-FL-sensor-expressing Tln1$^{-/-}$Tln2$^{-/-}$ cells with the Y-27632 compound, which reduces myosin-II activity. Similar to previously published integrin tension measurements[11], forces at aa 447 were lowered by Y-27632 treatment but did not seem to be entirely lost (**Fig. 4a**), probably because talin molecules within the remaining adhesion structures were still experiencing residual mechanical loads (**Supplementary Fig. 7a**). By contrast, forces at aa 1973 were abolished after addition of Y-27632 (**Fig. 4a**). We confirmed these observations with ratiometric imaging, in which individual Y-27632-treated cells were evaluated over time. Also in these experiments, tension at aa 447 was gradually

© 2017 Nature America, Inc., part of Springer Nature. All rights reserved.

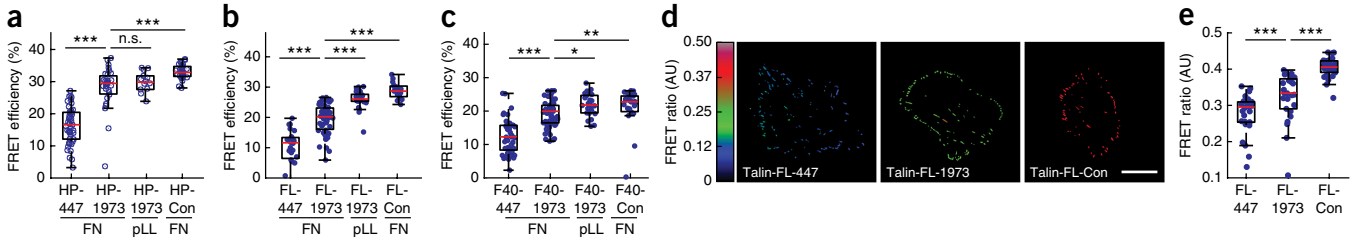

Figure 3 | Evaluating the intramolecular talin tension gradient. (**a**) FRET in talin-HP-1973-expressing cells is similar when cells are analyzed on fibronectin (FN)- and poly-L-Lysine (pLL)-coated glass slides (n = 45, 31, 31, 16 cells, pooled from five independent experiments). Talin-HP-Con cells display marginally higher FRET values on account of slightly increased intermolecular FRET[9]. (**b**) Live-cell FLIM analysis of FL-TSM-based talin sensors reveals significant tension at aa 1973 (n = 24, 59, 25, 17 cells, pooled from two to five independent experiments). (**c**) F40-TSM-based talin constructs confirmed decreased tension at aa 1973, but differences to pLL conditions were smaller (n = 41, 55, 26, 27 cells, pooled from four independent experiments). (**d**) Representative ratiometric FRET images of cells expressing talin-FL-447, talin-FL-1973, and talin-FL-Con; scale bar, 20 µm. (**e**) Mean FA-FRET as determined by ratiometric imaging (n = 26, 26, 26 cells, pooled from four independent experiments). (**a**–**c**,**e**: KS test; ***, $P < 0.001$; **, $P < 0.01$; *, $P < 0.05$; n.s., not significant, $P > 0.05$).

reduced, while forces at aa 1973 were lowered to control levels (**Fig. 4b,c** and **Supplementary Fig. 7b–d**).

As myosin-II activity is often positively correlated with FA size[25], we speculated that talin may experience mechanical tension at aa 1973 predominantly in large, mature FAs that are connected to contractile f-actin bundles. To test this hypothesis, we seeded cells onto two different micropatterned surfaces, upon which cells adapted very distinct morphologies (**Fig. 4d,e** and **Supplementary Fig. 8**). On triangular patterns cells displayed large and elongated FAs, strong peripheral stress fibers, and high myosin-II activity as indicated by myosin light chain phosphorylation (**Fig. 4d**). On disc-shaped micropatterns, cells formed mostly small FAs and displayed few stress fibers and little myosin-II activation (**Fig. 4e**). Consistent with our hypothesis, forces at aa 1973 were low in FAs of cells on round substrates but increased in large FAs of cells on triangular patterns (**Fig. 4f,g** and **Supplementary Fig. 9**).

The talin-1 tension gradient is vinculin dependent and sensitive to extracellular rigidity

We then tested how the presence of talin's binding partner vinculin affects the intramolecular tension gradient by expressing talin-FL-447 and talin-FL-1973 in vinculin-positive ($Vin^{f/f}$) or vinculin-deficient ($Vin^{-/-}$) fibroblasts. As expected, we observed different talin force values at aa 447 and aa 1973 in $Vin^{f/f}$ cells, similar to experiments in reconstituted $Tln1^{-/-}Tln2^{-/-}$ cell lines. By contrast, FRET efficiency differences were virtually absent in $Vin^{-/-}$ cells (**Fig. 4h**) because forces at aa 447 were markedly reduced. Thus, the intramolecular talin tension gradient is vinculin dependent.

Tension at aa 1973 was insensitive to vinculin expression, and this indicated that the low forces observed at the C-terminal region of talin are mediated by ABS3. To provide direct evidence for this, we generated talin-ABS3-deletion constructs and analyzed

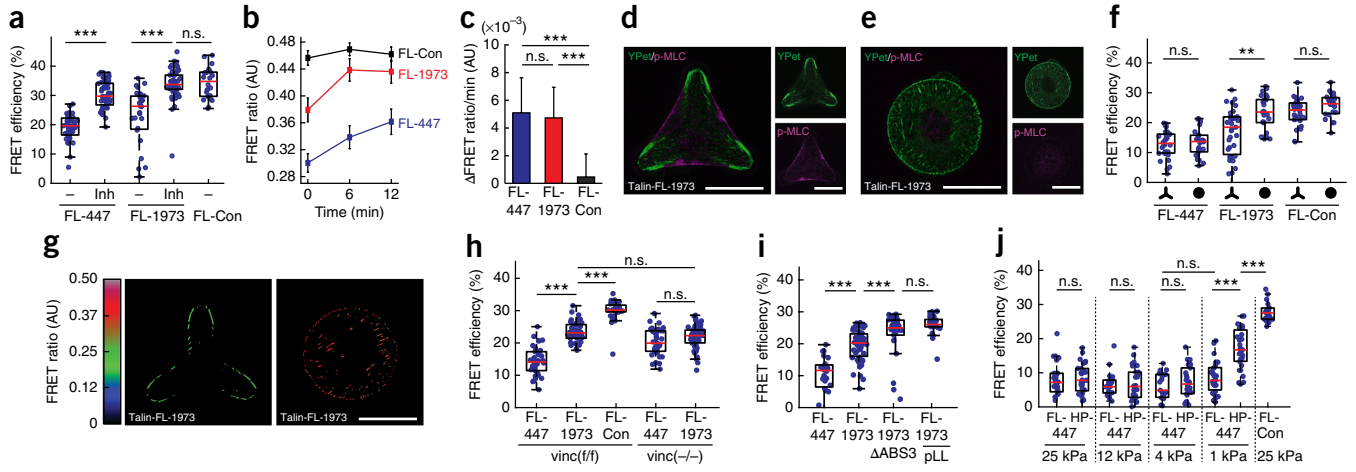

Figure 4 | Regulation of the intramolecular force gradient across talin. (**a**) FRET efficiencies in FAs of cells expressing distinct talin constructs before and after Y-27632 treatment (n = 49, 51, 37, 54, 22 cells, pooled from three independent experiments). (**b**) Mean FRET ratio change after Y-27632 treatment (n = 14, 16, 11 cells, pooled from five experiments). (**c**) Evaluation of FRET ratio change per minute reveals significant increase in FRET after Y-27632 treatment for talin-FL-447 and talin-FL-1973; FRET in talin-FL-Con cells is unaffected. (**d**,**e**) Representative cell seeded on a triangular or disc-shaped micropatterned substrate. Phosphorylated myosin light chain (p-MLC) signal is shown in magenta; the talin signal is displayed in green. (**f**) FA-FRET efficiencies in cells seeded on micropatterned substrates (n = 32, 27, 35, 27, 30, 23 cells, pooled from four experiments). (**g**) Representative FRET ratio image of a talin-FL-1973 cell seeded on a triangular or disc-shaped pattern. (**h**) Live-cell FRET analysis of talin-FL-447 and talin-FL-1973 expressed in $Vinc^{f/f}$ or $Vinc^{-/-}$ fibroblasts (n = 34, 42, 36, 40, 51 cells, pooled from four independent experiments). (**i**) Deletion of ABS3 leads to loss of tension at aa 1973 (talin-FL-1973-ΔABS3 n = 34, pooled from three experiments; other data as in **Fig. 3b**). (**j**) Live-cell FLIM analysis of cells expressing talin-FL-447 and talin-FL-1973 on FN-coated substrates with distinct rigidities (n = 29, 29, 20, 27, 19, 26, 31, 31, 20 cells, pooled from six independent experiments). (**a**, **c**, **f**, **h**–**j** KS test; ***, $P < 0.001$; *, $P < 0.05$; n.s., not significant, $P > 0.05$). Scale bars, 20 µm.

© 2017 Nature America, Inc., part of Springer Nature. All rights reserved.

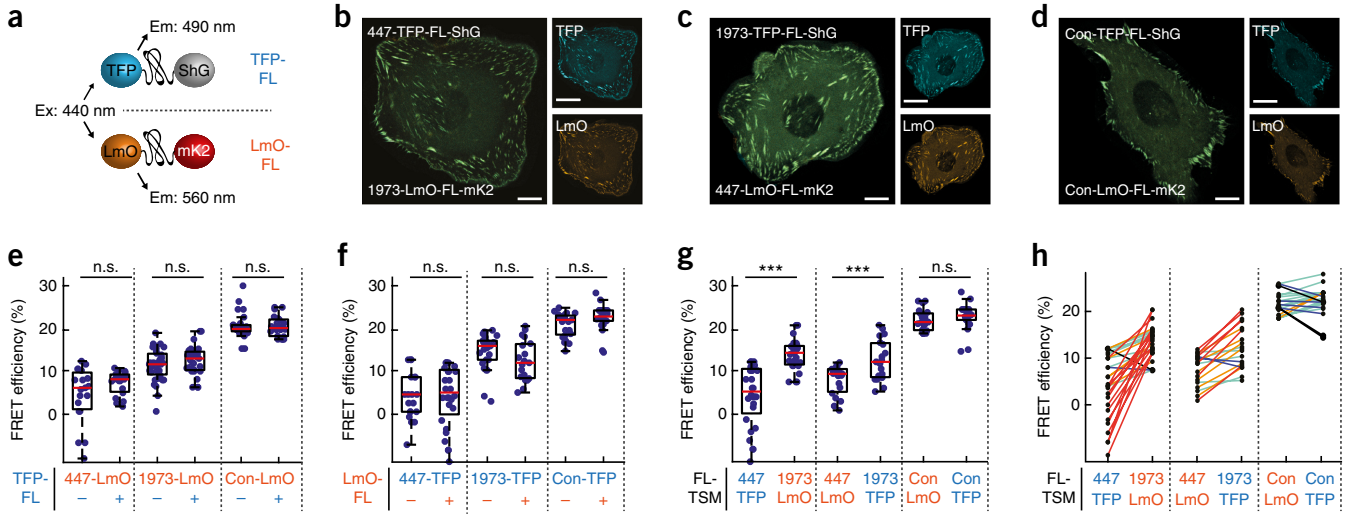

Figure 5 | Tension sensor multiplexing. (**a**) Schematic illustration of two orthogonal TSMs; both constructs are excitable by 440-nm light, but their emission wavelengths can be separated spectrally. (**b**,**c**) Stable coexpression of two orthogonal FL-based talin sensors (talin-FL-447 and talin-FL-1973); the constructs display indistinguishable subcellular localization. (**d**) Stable coexpression of two orthogonal talin control constructs (talin-FL-Con) showing identical subcellular localization. (**e**) Live-cell FLIM analysis of the LmO-FL-based talin sensors in the presence or absence of TFP-FL-based talin sensors (n = 19, 19, 35, 29, 26, 22 cells, pooled from six independent experiments). (**f**) Live-cell FLIM analysis of the TFP-FL-based talin sensors in the presence or absence of the LmO–FL construct (n = 19, 29, 26, 19, 27, 22 cells, pooled from six independent experiments). (**g**) Live-cell, dual-color FLIM confirms the intramolecular tension gradient across talin-1 (n = 29, 19, 22 cells, pooled from six independent experiments). (**h**) Visualization of corresponding FRET efficiency values from individual cells (same data as shown in **g**). Red colors indicate a steep tension differential; black colors indicate its absence. (**e**,**f**, KS test; **g**, paired t-test; ***, $P < 0.001$; n.s., not significant, $P > 0.05$). Scale bars, 20 µm.

© 2017 Nature America, Inc., part of Springer Nature. All rights reserved.

them in Tln1$^{-/-}$Tln2$^{-/-}$ cells. As previously observed[26], ABS3-deficient constructs only partially rescued the spreading defect of talin-deficient cells (**Supplementary Fig. 10**), and we focused the analysis on cells that did form FAs. These experiments revealed strongly increased FRET values, which suggested that an intact ABS3 is required for tension at aa 1973 (**Fig. 4i**). Finally, we investigated how talin mechanics are affected by the stiffness of the extracellular substrate. While forces at aa 1973 remained rather constant and comparable to those measured on glass slides, talin-HP-447 experiments revealed reduced tension at N-terminal parts of the rod domain on soft, 1-kPa surfaces (**Fig. 4j** and **Supplementary Fig. 11**).

Together, these experiments demonstrate that the intramolecular tension gradient across talin-1 can be modulated at the N- and C-terminal parts of the talin rod domain. The tension differential is controlled by f-actin binding and myosin activity; it is vinculin dependent, and it is sensitive to the stiffness of the extracellular substrate.

Orthogonal tension sensor module pairs allow tension sensor multiplexing by dual-color FLIM

A limitation of the described experiments was that the two biosensors were analyzed in parallel, but not within the same cell. We therefore generated two orthogonal TSMs, called multiplexing (MPX) TSMs, that could be imaged simultaneously using single-excitation wavelength, dual-color FLIM[27]. For the first MPX-TSM, we used mTFP1 as a donor and the dark quencher ShadowG as an acceptor[27,28]; for the second module, we combined the long Stokes shift (LSS) fluorophore LSSmOrange with mKate2 (refs. 27,29; **Fig. 5a**). Evaluation of the individual fluorophores and MPX-TSMs revealed a narrow fluorescence lifetime distribution of mTFP1 and LSSmOrange and similar, albeit not identical, FRET efficiencies of the respective MPX-TSMs (**Fig. 5** and **Supplementary Fig. 12a**). Coexpression of the corresponding multiplexing talin-FL-447, talin-FL-1973, and control constructs in Tln1$^{-/-}$Tln2$^{-/-}$cells demonstrated normal subcellular localization (**Fig. 5b–d**). Consistent with the experiments above, we observed low FRET values for talin-FL-447 and higher transfer rates for talin-FL-1973 constructs. Notably, results did not depend on the choice of TSM or whether cells expressed just one or both constructs, demonstrating that the MPX-TSMs can indeed be used orthogonally (**Fig. 5e,f** and **Supplementary Fig. 12b**). Simultaneous evaluation by dual-color FLIM confirmed these observations. As two distinct fluorophore pairs were used, differences in FRET efficiency were not identical, but the overall tendencies were consistently reproduced (**Fig. 5g,h**). Of note, some lifetime values were unusually high, and this resulted in negative FRET values, probably a consequence of reduced FRET efficiency in MPX-TSM constructs and the normal spread in the data. The negative FRET efficiencies may also indicate less efficient folding or chromophore maturation in the employed fluorophores; thus, future studies may be directed toward optimizing orthogonal FRET pairs with increased FRET efficiencies and efficient maturation rates. Yet, the observations were consistent with the experiments in which TSMs were analyzed separately (**Figs. 3** and **4**) and so provided direct evidence for an intramolecular force gradient across talin.

Calculating the fraction of mechanically engaged talin molecules using FL-TSM

Given the virtually digital nature of FL-TSM (**Fig. 1**) as well as the observed differences between talin-FL-447 and talin-FL-1973 (**Fig. 3**), the data indicated that only a fraction of FA-localized talin molecules experiences mechanical forces of more than 3 pN at talin's C-terminal region. To estimate this fraction, we

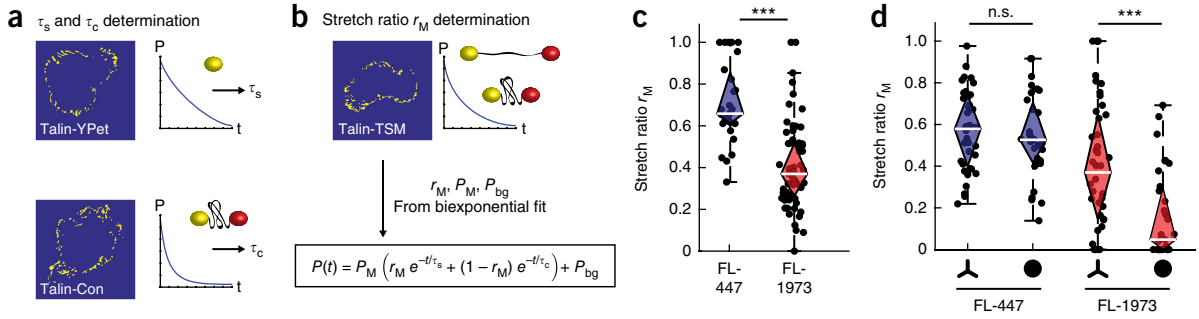

Figure 6 | Estimating the molecular engagement ratio. (**a**) Fluorescence lifetimes of stretched (s) and closed (c) sensor molecules τ_s and τ_c can be experimentally determined from cells expressing talin-YPet and talin-Con. (**b**) The biexponential fit of the photon count $P(t)$ can be performed with τ_s and τ_c and used to calculate the photon count rates of biosensor (P_M) and background (P_{bg}) as well as the molecular stretch ratio r_M. (**c**) Evaluating the molecular engagement ratio using FLIM data from cells expressing talin-FL-447 and talin-FL-1973 (same experiment as in **Fig. 3b**; n = 27, 64 cells, pooled from two to five independent experiments). (**d**) Evaluating the molecular engagement ratio using the FLIM data shown in **Figure 4f** (n = 36, 31, 42, 31 cells, pooled from four independent experiments). (**c**,**d**: Mann–Whitney U test; ***, $P < 0.001$; n.s., not significant, $P > 0.05$).

determined the fluorescence donor lifetime of FL-TSM in the stressed state (corresponding to the donor-only lifetime) and unstressed state (lifetime of talin-Con), and we used these values when fitting a biexponential decay function to the talin-FL-447 and talin-FL-1973 lifetime data (**Fig. 6a,b**). An estimation of the minimum amount of photon counts necessary for statistically reliable calculations indicated that about 10,000 photons are required (**Supplementary Fig. 13**), a number that is surpassed in our experiments. Consistent with the assumption that the FL-based sensors essentially exist in two states (high FRET and no FRET), the data were well described by the biexponential function, as indicated by the Pearson's chi-squared test (talin-FL-447, ~0.43; talin-FL-1973, ~0.46).

Evaluation of FLIM data sets from adherent cells showed that about 70% of talin molecules are exposed to tension at aa 447, while only about 40% of talin molecules experience mechanical loads at aa 1973 (**Fig. 6c**). As expected, evaluation of micropatterning data sets demonstrated that the fraction of molecules bearing tension at aa 1973 is higher in cells on triangular patterns as compared to conditions of low intracellular contractility (**Fig. 6d**). Together, the results imply that cells not only modulate the amount of force per molecule but also adjust the number of talin molecules mechanically engaged through ABS3.

DISCUSSION

This study establishes a powerful method to quantify molecular pN-scale forces within cells. FL-TSM benefits from a sharp force response that allows quantitative interpretation of ensemble measurements in the low-pN force regime at 3–5 pN. In comparison with the widely used F40-based construct[8], FL-TSM exceled because of an improved FRET efficiency at zero-force and enlarged contour length increase under tension, resulting in an increased dynamic range. Most importantly, the near-digital force response characteristic of FL-TSM can be harnessed to estimate the fraction of mechanically engaged molecules from FLIM-based ensemble measurements.

In addition, we established a method to quantify two intracellular tension sensor constructs simultaneously. The tension sensor multiplexing technique can be used to determine pN-scale forces across different domains of individual proteins, but it should be particularly valuable for studying the molecular mechanics of two distinct molecules that may or may not reside in the same subcellular structure.

When applied to talin, these tools revealed an intramolecular tension gradient characterized by comparatively high forces of more than 7 pN at the N-terminal part of the talin rod domain and lower tension at the C-terminal talin region between ABS2 and ABS3. We thus conclude that the previously described force-induced vinculin binding is likely to occur primarily at N-terminal regions of the talin rod domain[30,31], and it will be interesting to study how the described tension differential across talin affects the overall mechanics of cell adhesion. The implementation of a tension gradient into the molecular clutch model of FAs[32,33] or similar theoretical frameworks[34] seems especially important, because the presented data demonstrate that integrin force transduction through talin is regulated on at least two levels. First, talin molecules are exposed to a range of forces that are typically above 7 pN in the N-terminal part of the molecule and lower than 7 pN in C-terminal regions. Second, cells tune how many talin molecules are mechanically engaged. Both modes of regulation are sensitive to vinculin binding, f-actin association, and myosin-II activity; and the recent identification of additional talin interactors suggests additional layers of modulation[35,36].

Altogether, the data show that experimentally addressing molecular mechanisms of force transduction requires a set of calibrated tension sensors to investigate the whole range of forces experienced by molecules in cells as well as advanced data analysis tools to study proteins' engagement ratio. The methods described above should be valuable for these studies and adaptable to a wide range of research questions.

METHODS

Methods, including statements of data availability and any associated accession codes and references, are available in the online version of the paper.

Note: Any Supplementary Information and Source Data files are available in the online version of the paper.

ACKNOWLEDGMENTS

The authors thank R. Fässler (MPI of Biochemistry, Department of Molecular Medicine) for providing talin-deficient cells, C. Schweizer for help with programming, the MPIB core facility for technical support, and the Microscopy Rennes Imaging Centre (MRic), where multiplex FRET experiments were

© 2017 Nature America, Inc., part of Springer Nature. All rights reserved.

performed. C.G. is supported by the German Research Council (DFG, GR3399/5-1 and GR3399/6–1), the Collaborative Research Centre SFB863 (B9), and the Max Planck Förderstiftung. M.R. acknowledges support from the German Research Council through the Collaborative Research Centre SFB863 (A2), and M.T. acknowledges funding by the Ligue Régionale Contre le Cancer. A.F. was supported by the Boehringer Ingelheim Fonds.

AUTHOR CONTRIBUTIONS

P.R. generated expression constructs and cell lines, performed experiments, wrote data analysis software, and analyzed data. A.W. performed calibration experiments, data analysis, and theoretical modeling with A.M. under the supervision of M.R. A.-L.C. wrote FLIM analysis software and advanced data analysis algorithms with assistance from B.S. A.F. generated tools and performed initial experiments. M.T. provided multiplexing fluorophores and supervised dual-colour FLIM experiments and data analysis. C.G. purified TSMs, coordinated experiments, and wrote the manuscript with input from all authors.

COMPETING FINANCIAL INTERESTS

The authors declare no competing financial interests.

Reprints and permissions information is available online at http://www.nature.com/reprints/index.html. Publisher's note: Springer Nature remains neutral with regard to jurisdictional claims in published maps and institutional affiliations.

1. Petridou, N.I., Spiró, Z. & Heisenberg, C.P. Multiscale force sensing in development. *Nat. Cell Biol.* **19**, 581–588 (2017).
2. Vogel, V. & Sheetz, M. Local force and geometry sensing regulate cell functions. *Nat. Rev. Mol. Cell Biol.* **7**, 265–275 (2006).
3. Gordon, W.R. *et al.* Mechanical allostery: evidence for a force requirement in the proteolytic activation of notch. *Dev. Cell* **33**, 729–736 (2015).
4. Rognoni, L., Stigler, J., Pelz, B., Ylänne, J. & Rief, M. Dynamic force sensing of filamin revealed in single-molecule experiments. *Proc. Natl. Acad. Sci. USA* **109**, 19679–19684 (2012).
5. del Rio, A. *et al.* Stretching single talin rod molecules activates vinculin binding. *Science* **323**, 638–641 (2009).
6. Buckley, C.D. *et al.* Cell adhesion. The minimal cadherin-catenin complex binds to actin filaments under force. *Science* **346**, 1254211 (2014).
7. Finer, J.T., Simmons, R.M. & Spudich, J.A. Single myosin molecule mechanics: piconewton forces and nanometre steps. *Nature* **368**, 113–119 (1994).
8. Grashoff, C. *et al.* Measuring mechanical tension across vinculin reveals regulation of focal adhesion dynamics. *Nature* **466**, 263–266 (2010).
9. Austen, K. *et al.* Extracellular rigidity sensing by talin isoform-specific mechanical linkages. *Nat. Cell Biol.* **17**, 1597–1606 (2015).
10. Wang, X. & Ha, T. Defining single molecular forces required to activate integrin and notch signaling. *Science* **340**, 991–994 (2013).
11. Zhang, Y., Ge, C., Zhu, C. & Salaita, K. DNA-based digital tension probes reveal integrin forces during early cell adhesion. *Nat. Commun.* **5**, 5167 (2014).
12. Morimatsu, M., Mekhdjian, A.H., Chang, A.C., Tan, S.J. & Dunn, A.R. Visualizing the interior architecture of focal adhesions with high-resolution traction maps. *Nano Lett.* **15**, 2220–2228 (2015).
13. Freikamp, A., Cost, A.L. & Grashoff, C. The piconewton force awakens: quantifying mechanics in cells. *Trends Cell Biol.* **26**, 838–847 (2016).
14. Borghi, N. *et al.* E-cadherin is under constitutive actomyosin-generated tension that is increased at cell–cell contacts upon externally applied stretch. *Proc. Natl. Acad. Sci. USA* **109**, 12568–12573 (2012).
15. Chang, C.W. & Kumar, S. Vinculin tension distributions of individual stress fibers within cell–matrix adhesions. *J. Cell Sci.* **126**, 3021–3030 (2013).
16. Krieg, M., Dunn, A.R. & Goodman, M.B. Mechanical control of the sense of touch by β-spectrin. *Nat. Cell Biol.* **16**, 224–233 (2014).
17. Paszek, M.J. *et al.* The cancer glycocalyx mechanically primes integrin-mediated growth and survival. *Nature* **511**, 319–325 (2014).
18. Hernández-Varas, P., Berge, U., Lock, J.G. & Strömblad, S. A plastic relationship between vinculin-mediated tension and adhesion complex area defines adhesion size and lifetime. *Nat. Commun.* **6**, 7524 (2015).
19. Sun, Z., Guo, S.S. & Fässler, R. Integrin-mediated mechanotransduction. *J. Cell Biol.* **215**, 445–456 (2016).
20. Fang, J. *et al.* Forced protein unfolding leads to highly elastic and tough protein hydrogels. *Nat. Commun.* **4**, 2974 (2013).
21. Dietz, H. & Rief, M. Exploring the energy landscape of GFP by single-molecule mechanical experiments. *Proc. Natl. Acad. Sci. USA* **101**, 16192–16197 (2004).
22. Critchley, D.R. Biochemical and structural properties of the integrin-associated cytoskeletal protein talin. *Annu. Rev. Biophys.* **38**, 235–254 (2009).
23. Calderwood, D.A., Campbell, I.D. & Critchley, D.R. Talins and kindlins: partners in integrin-mediated adhesion. *Nat. Rev. Mol. Cell Biol.* **14**, 503–517 (2013).
24. Mehlich, A., Austen, K., Ringer, P., Rief, M. & Grashoff, C. Evaluation of molecular tension sensors using single-molecule force spectroscopy and live cell FRET imaging. *Protocol Exchange* http://dx.doi.org/10.1038/protex.2015.095 (2015).
25. Geiger, B., Spatz, J.P. & Bershadsky, A.D. Environmental sensing through focal adhesions. *Nat. Rev. Mol. Cell Biol.* **10**, 21–33 (2009).
26. Atherton, P. *et al.* Vinculin controls talin engagement with the actomyosin machinery. *Nat. Commun.* **6**, 10038 (2015).
27. Demeautis, C. *et al.* Multiplexing PKA and ERK1&2 kinases FRET biosensors in living cells using single excitation wavelength dual colour FLIM. *Sci. Rep.* **7**, 41026 (2017).
28. Murakoshi, H., Shibata, A.C.E., Nakahata, Y. & Nabekura, J. A dark green fluorescent protein as an acceptor for measurement of Förster resonance energy transfer. *Sci. Rep.* **5**, 15334 (2015).
29. Shcherbakova, D.M., Hink, M.A., Joosen, L., Gadella, T.W.J. & Verkhusha, V.V. An orange fluorescent protein with a large Stokes shift for single-excitation multicolor FCCS and FRET imaging. *J. Am. Chem. Soc.* **134**, 7913–7923 (2012).
30. Yao, M. *et al.* The mechanical response of talin. *Nat. Commun.* **7**, 11966 (2016).
31. Haining, A.W.M., von Essen, M., Attwood, S.J., Hytönen, V.P. & Del Río Hernández, A. All subdomains of the talin rod are mechanically vulnerable and may contribute to cellular mechanosensing. *ACS Nano* **10**, 6648–6658 (2016).
32. Chan, C.E. & Odde, D.J. Traction dynamics of filopodia on compliant substrates. *Science* **322**, 1687–1691 (2008).
33. Elosegui-Artola, A. *et al.* Mechanical regulation of a molecular clutch defines force transmission and transduction in response to matrix rigidity. *Nat. Cell Biol.* **18**, 540–548 (2016).
34. Besser, A. & Safran, S.A. Force-induced adsorption and anisotropic growth of focal adhesions. *Biophys. J.* **90**, 3469–3484 (2006).
35. Bouchet, B.P. *et al.* Talin-KANK1 interaction controls the recruitment of cortical microtubule stabilizing complexes to focal adhesions. *eLife* **5**, e18124 (2016).
36. Sun, Z. *et al.* Kank2 activates talin, reduces force transduction across integrins and induces central adhesion formation. *Nat. Cell Biol.* **18**, 941–953 (2016).

© 2017 Nature America, Inc., part of Springer Nature. All rights reserved.

© 2017 Nature America, Inc., part of Springer Nature. All rights reserved.

ONLINE METHODS

Protocol. A detailed protocol on single-molecule force spectroscopy calibration of FRET-based tension sensors and time-correlated single-photon counting (TCSPC)-FLIM analysis is available in *Protocol Exchange*[24].

Antibodies and reagents. The following antibodies and reagents were used: anti-vinculin (hVIN-1) (V9131, Sigma; IF 1:200), anti-paxillin (610051, BD Transduction L.; IF 1:400), anti-p-MLC (Ser19) (3671, NEB; IF 1:50), anti-mouse IgGAlexa Fluor-405 (A31553; IF 1:400; Thermo Fisher Scientific), Alexa Fluor-647 phalloidin (A22287; IF 1:200; Thermo Fisher Scientific), poly-L Lysine (P4707; Sigma), fibronectin (341631; Calbiochem), puromycin (P8833; Sigma), hygromycin B (H3274; Sigma). Micropatterned substrates (10-011-00-18, 10-002-10-18; CYTOO), softview Easy Coat substrate dishes: 1.0, 4.0, 12 and 25 kPa dishes (Matrigen), Y-27632 (Y0505, Sigma).

Plasmid construction. The cDNA of TSMs as well as talin biosensors was constructed according to our published protocols[37]. Plasmids will be distributed through AddGene (http://www.addgene.org/). Complete plasmid information is available through Genbank using the following accession codes: HP35-TSM (MF685010), F40-TSM (MF685012) and FL-TSM (MF685013).

Generation of FL-TSM. To generate the FL-based TSM, restriction sites were added to the cDNA of YPet (aa 1–228) (5Xho/3′BamHI) and mCherry (5′BamHI/3′NotI) by polymerase chain reaction (PCR), and PCR products were combined in pBluescript SK(+). The cDNA sequence encoding for the FL peptide (MGE FDI RFR TDD DEQ FEK VLK EMN RRA RKD AGT VTY TRD GND FEI RIT GIS EQN RKE LAK EVE RLA KEQ NIT VTY TER GSL E) was synthesized (5′-ATG GGC GAG TTT GAC ATC CGG TTT CGG ACT GAT GAC GAC GAA CAG TTC GAG AAA GTG CTG AAG GAG ATG AAT CGT CGA GCC AGA AAG GAT GCT GGA ACT GTG ACC TAC ACA AGG GAT GGG AAT GAC TTC GAG ATT CGC ATT ACC GGC ATA AGC GAG CAA AAC CGC AAA GAA CTG GCC AAA GAG GTT GAA AGG CTT GCA AAG GAA CAG AAC ATC ACA GTC ACG TAT ACC GAG AGA GGT TCC CTC GAA-3′; Eurofins Genomics) and inserted between the fluorophore cDNAs using 5′BglII/3′BamHI overhangs; this FL-TSM cDNA was then transferred into the pLPCX expression plasmid (Clontech). For single-molecule force spectroscopy calibration, terminal cysteine residues to allow attachment of DNA oligonucleotides and a histidine tag for protein purification were added. mTFP1–ShadowG and LSSmOrange–mKate2 constructs were assembled in pLPCX by standard PCR and Gibson assembly (Gibson Assembly Cloning Kit; New England Biolabs). All sequences were confirmed by DNA sequencing (Eurofins Genomics).

Generation of talin expression constructs. Talin-TSM-447 and control cDNAs were generated according to the previously published strategy[9,37]. To insert the respective TSM at aa 1973 of talin-1 (i.e., talin-TSM-1973 constructs), we generated 5′XhoI/3′NotI restriction sites after aa 1973 using standard PCR and Gibson assembly. cDNAs were assembled in the pLPCX or pLHCX vectors, and the correct sequence of constructs was confirmed by DNA sequencing. C-terminal fusion constructs were cloned by assembling the PCR products of the respective TSM or fluorophores using 3′ClaI/5′NotI restriction sites that were inserted after the cDNA of talin-1.

FL-sensor module expression and purification. For FL-TSM and F40-TSM protein expression, HEK293 cells were transfected by $CaPO_4$-precipitation. After 48 h, cells were detached, resuspended in hypotonic lysis buffer (20 mM Tris, 2 mM $MgCl_2$, pH 7.4), incubated for 20 min on ice, and then lysed with a Dounce homogenizer. Cell lysates were cleared by 10 min centrifugation at 4 °C and purified by metal ion affinity chromatography (His-Trap; GE Healthcare), followed by ion-exchange chromatography (Sephadex; GE Healthcare). Purified samples were then concentrated to about 20 µM by membrane ultrafiltration (Vivaspin; GE Healthcare) and stored at −80 °C in phosphate buffered saline (PBS; pH 6.7) supplemented with 0.2 mM Tris-2-carboxyethylphosphine (TCEP) to avoid oligomerization via terminal cysteines.

Assembling protein–DNA conjugates. To attach DNA handles to the purified FL-TSM, lyophilized maleimide-modified single-stranded (ss) DNA oligonucleotides were dissolved in PBS (pH 6.7) and incubated with the purified protein for 1 h at room temperature (RT). Unreacted components were removed using metal ion affinity chromatography (His-Trap, GE Healthcare) and size-exclusion chromatography (Superdex 200; GE Healthcare). Next, 185 nm long, double stranded (ds) DNA handles (λ-DNA; NEB) carrying a biotin or a digoxigenin modification and a complementary ss overhang were hybridized with the protein–DNA chimera. The sample was then prepared by incubating streptavidin-coated 1 µm sized silica beads (Bangs Laboratories) with the protein–DNA chimeras for 5 min in PBS (pH 7.4). Functionalized antidigoxigenin silica beads were added subsequently; glucose oxidase and catalase were used as an oxygen scavenger system. Finally, one of each bead species was caught in the two traps and moved in close proximity to allow tether formation. Then the protein was unfolded and refolded in stretch–relax cycles by periodically changing the trap distance with constant velocity. For equilibrium measurements, traps held at constant distance and bead positions were recorded during unfolding and refolding.

Single-molecule force spectroscopy calibration. Single-molecule force spectroscopy measurements were performed on a custom-built, dual-trap optical tweezers setup with back focal plane detection as described before[24,38]. In short, excitation light of a diode pumped Nd:YVO_4 laser (Spectra Physics) was split into two beams by a polarizing beam splitter. A piezo mirror stage (Mad City Labs) was used to laterally displace one beam in the sample plane. A second polarizing beam splitter was installed to combine and focus both beams onto the sample plane by a microscope objective (63×/1.20 W Corr, C-Apochromat; Zeiss). To monitor bead displacement, the forward-scattered light was collected by an identical objective, and the back focal plane was imaged by quadrant photo diodes (QP154-Q-HVSD, First Sensor). The calibration of trap stiffness and detector sensitivity was performed as described earlier[39]; the signals were detected at 150 kHz and averaged to 30 kHz before storage. To improve resolution, analysis was performed on the difference of the two signals as described[40].

Calibration data analysis. Singe-molecule data analysis followed the procedures described before[9,24]. To extract the mechanical properties of the dsDNA handles, an extensible worm-like chain model (eWLC)[41] was fit to the measured force–extension data according to equation (1)

$$F_{\mathrm{eWLC}}(x_{\mathrm{DNA}}, L_{\mathrm{DNA}}, p_{\mathrm{DNA}}, K) = \frac{k_B T}{p_{DNA}}\left[\frac{1}{4\left(1-\frac{x_{\mathrm{DNA}}}{L_{\mathrm{DNA}}}+\frac{F_{\mathrm{WLC}}}{K}\right)^2}+\frac{x_{\mathrm{DNA}}}{L_{\mathrm{DNA}}}-\frac{F_{\mathrm{WLC}}}{K}-\frac{1}{4}\right] \quad (1)$$

where x_{DNA} is the measured extension of the DNA tether; and L_{DNA}, p_{DNA}, and K are fit parameters that correspond to the contour length, the persistence length and the stretch modulus of the dsDNA handles. The temperature inside the measurement chamber was assumed to be T = 303 K. In our experiments, the average fit persistence length was 16.3 nm, the stretch modulus between 150–300 pN, and the averaged fit contour length 362.6 nm, values consistent with the expected length of 370 nm of the two dsDNA handles. For extracting the mechanical response parameters of the protein, a basic worm-like chain model was fitted in series with the eWLC to the data according to equation (2):

$$F_{\mathrm{WLC}}(x_p, L_p, p_p) = \frac{k_B T}{p_p}\left[\frac{1}{4\left(1-\frac{x_p}{L_p}\right)^2}+\frac{x_p}{L_p}-\frac{1}{4}\right] \quad (2)$$

where x_p is the measured protein extension, and L_p is the fitted protein contour length gain. The experimentally determined contour length gain was 27.4 ± 2.6 nm, which is in agreement with previously published data[20].

With the assumption that the dsDNA handles are at equilibrium with the unfolded protein, the acting forces can be set equal: $F_{\mathrm{eWLC}} = F_{\mathrm{WLC}} = F$. Thus, the total extension of the tether can be expressed according to equation (3):

$$x_{\mathrm{tether}}(F) = x_{\mathrm{DNA}}(F) + x_p(F)\cdot P_{\mathrm{unf}}(F) \quad (3)$$

$x_{\mathrm{DNA}}(F)$ and $x_p(F)$ being the extension of DNA handles and protein, and $P_{\mathrm{unf}}(F)$ being the unfolding probability. Inversion yields the force–extension correlation for the entire tether.

In the low-pN force regime, optical traps can be assumed to have a harmonic potential and follow the Hookean law according to

$$F(d) = k_{\mathrm{eff}}\cdot\langle x_{\mathrm{B}}\rangle \quad (4)$$

where

$$k_{\mathrm{eff}} = \left(\frac{1}{k_1}+\frac{1}{k_2}\right)^{-1}$$

is the effective trap stiffness, and $x_B = x_{B1} + x_{B2}$ the displacement of the two beads from the respective trap centers. The extension of the tethered construct x_{tether} can be calculated by subtracting the sum of bead displacement $x_{B1} + x_{B2}$ and twice the bead diameter R from the distance of the trap centers d

$$x_{\mathrm{tether}} = d - (2R + x_{B1} + x_{B2}) \quad (5)$$

The mean displacement can be expressed as

$$\langle x_B\rangle = \int_{-\infty}^{+\infty} dx_B x_B \cdot p(x_B) \quad (6)$$

where $p(x_B)$ is the Boltzmann probability distribution

$$p(x_B) = \frac{1}{Z}\cdot\exp\left(-\frac{H(x_B)}{k_B T}\right) \quad (7)$$

with the canonical partition function

$$Z = \int_{-\infty}^{+\infty} dx_B \exp\left(-\frac{H(x_B)}{k_B T}\right)$$

and the Hamiltonian

$$H(x,i) = (1-i)\cdot\Delta G^0 + \frac{1}{2}k_{\mathrm{eff}}x^2 + \int_0^{d-x} dx_{\mathrm{tether}} F_{\mathrm{tether}}(i\cdot L_p, x_{\mathrm{tether}} \quad (8)$$

with i representing the number of unfolded subunits, and F_{tether} being the inversion of equation (3). As FL-TSM is a two-state folder, $i \in \{0,1\}$, the force–distance relation given by equation (4) is hence described by

$$F(d) = \frac{k_{\mathrm{eff}}}{\int_{-\infty}^{+\infty} dx \sum_{i=0}^{1}\exp\left(\frac{H(x,i)}{k_B T}\right)}\cdot\int_{-\infty}^{+\infty} dx\, x\cdot\sum_{i=0}^{1}\exp\left(\frac{H(x,i)}{k_B T}\right) \quad (9)$$

The force–distance relation (equation (9)) depends only on the Hamiltonian $H(x,i)$ (equation (8)). Thus, the free parameters are x_{tether}, which is a directly measured quantity; L_p, which is obtained by fitting constant velocity traces according to equation (2); and the folding free energy ΔG^0.

Free energy calculation from constant distance measurements. In contrast to our previous study[9], ΔG^0 was determined from passive, constant distance measurements. In this mode, the trap distance is kept constant, and iterative unfolding and refolding events are observed over time. A hidden Markov (HM) analysis was performed on the raw data as described before[42] to assign a state to each recorded data point. The time trajectories were coarse grained in 100 bins to facilitate numerical calculations. To initialize the HM analysis, emission probabilities, which reflect the deflection distribution of each state, were retrieved from Gaussian fits to a histogram of the respective time trajectory.

The force-dependent folding and unfolding probabilities $P_{\mathrm{fold}}(F)$ and $P_{\mathrm{unf}}(F)$ (**Fig. 1d** and **Supplementary Fig. 2b**) and thus the relative amount of time of the FL-TSM spent in the folded and unfolded states were sampled by recording traces at different trap distances (**Fig. 1c**). The total energy in the system $G_i(F_i)$ at a given force F_i in state i is described by equation (10):

$$G_i(F_i) = G_i^0 + G_i^{\mathrm{device}} = G_i^0 + G_i^{\mathrm{bead}}(F_i) + G_i^{\mathrm{DNA}}(F_i) + G_i^p(F_i) \quad (10)$$

© 2017 Nature America, Inc., part of Springer Nature. All rights reserved.

doi:10.1038/nmeth.4431

where G_i^0 is the free energy of the protein in state i;

$$G_i^{\text{bead}}(F_i)=\frac{1}{2}x_B(F_i)\bullet F_i$$

the energy stored in bead deflection x_B. G_i^{DNA} and G_i^p correspond to the energy stored in the stretched DNA and polypeptide chain. The free energy difference between two states i and j is given by

$$\Delta G_{ij}\left(F_i,F_j\right)=\Delta G_{ij}^0+\Delta G_{ij}^{\text{device}}\left(F_i,F_j\right) \quad (11)$$

The free energy difference of the protein states ΔG_{ij}^0 was obtained by performing a global fit to the force-dependent probabilities according to equation (12):

$$P_i(F)=\frac{1}{1+\sum_{i\neq j}\exp\left(-\frac{\Delta G_{ij}^0}{k_BT}+\frac{\Delta G_{ij}^{\text{device}}\left(F,F_j\right)}{k_BT}\right)} \quad (12)$$

The obtained free energy difference ΔG_0 for FL-TSM was 4.3 ± 1 k_BT.

Calculating the FRET efficiency-force correlation. The FRET–force correlation, depicted in **Figure 1f**, can be calculated by

$$E_{\text{FRET}}(F)=E_{\text{FRET}}\left(x_p^{\text{fold}}\right)\cdot P_{\text{fold}}(F)+E_{\text{FRET}}\left(x_{\text{p}}^{\text{unf}}(F)\right)\cdot P_{\text{unf}}(F) \quad (13)$$

$E_{\text{FRET}}\left(x_p^{\text{fold}}\right)$ corresponds to the FRET efficiency when the sensor protein is still folded (**Supplementary Fig. 2a,c**). This FRET efficiency was about 29% in our live-cell experiments (**Fig. 1i**), which corresponds to a fluorophore separation distance of approximately 6.7 nm.

Calculating the tension sensor model sensitivity. The sensitivity of the TSMs is defined as the absolute slopes of the FRET–force relation (equation (13)). Obtained sensitivity curves were multiplied with a normalization constant, which sets the maximum of the first reported TSM, F40-TSM, equal to one. The full width at half maximum of each curve serves as a measure of the digital nature of the sensor (**Fig. 1g**).

Single-molecule measurements with the F40-TSM. For calibration of F40-TSM, single-molecule force experiments were conducted as with FL-TSM, meaning DNA handles were attached to N and C termini, and stretch–relax traces were recorded. As expected, no distinct unfolding event could be observed, owing to the nano-spring-like properties of the F40 peptide[8] (**Supplementary Fig. 1a,b**). Therefore, at the end of each experiment, the construct was stretched to 40–55 pN to unfold the fluorophores and to ensure that a functional F40-TSM construct had been trapped (**Supplementary Fig. 1a**). The additional length gain arising from stretching the F40 peptide can be measured indirectly. The contour length of the entire tether of the F40-TSM calibration construct (i.e., the F40-TSM protein plus the DNA handles) was compared to the contour length of the entire tether of the folded FL-TSM calibration construct (**Supplementary Fig. 1b**). The observed differences correspond to the extension of the F40 peptide, and a Gaussian fit of these data yielded a mean contour length increase of 10.6 ± 5.9 nm for F40-TSM (**Supplementary Fig. 1c**). Of note, this type of measurement yields a much broader probability density histogram when compared to direct contour length measurement (as done for FL-TSM, HP35st-TSM, and HP35-TSM). However, previously published force-FRET-efficiency data[8] were reproduced well with the model described above and the experimentally determined F40-TSM contour length of about 10.6 nm (data not shown). Thus, a conversion of the force–FRET correlation, which matches the zero-force FRET efficiency of theYPet–mCherry construct used here, could be calculated.

Cell culture conditions and expression of FRET constructs. All cell lines (i.e., Tln1$^{-/-}$Tln2$^{-/-}$cells, Vin$^{f/f}$ cells, Vin$^{-/-}$ cells, and HEK293 cells) were cultured in high-glucose DMEM-GlutaMAX medium (Thermo Fisher Scientific) supplemented with 10% fetal bovine serum (FBS; Thermo Fisher Scientific) and 1% penicillin/streptomycin (P/S; Thermo Fisher Scientific). For live-cell imaging, DMEM without phenol red containing 4.5 mg/ml glucose, 25 mM HEPES, 2 mM glutamine (Thermo Fisher Scientific) supplemented with 10% FBS and 1% P/S was used. Stable cell lines were established by using the phoenix cell transfection system. Ecotropic, retroviral particles were produced according to established protocols[37], and target cells were infected in the presence of 5 µg/ml polybrene. After five infection cycles, cells were selected with puromycin or hygromycin depending on the expression vector used. For transient expression, cells were transduced with Lipofectamine 2000 (Invitrogen).

Immunostaining and isolation of focal-adhesion-specific signal. For immunostaining and FA analysis, cells were seeded on no. 1.5 glass slides (Menzel) coated with 10 µg/ml FN. Cells were allowed to spread overnight (O/N), then they were fixed with 4% paraformaldehyde (PFA) for 10 min at RT and washed in PBS (pH 7.4). Immunostainings were performed using standard protocols and antibody concentrations indicated above. Samples were then washed in PBS, mounted in Prolong Gold antifade mountant (Thermo Fisher Scientific) and stored at 4 °C. Images were acquired using a LSM780 confocal scanning microscope (Zeiss) equipped with a 100× oil objective (Plan-APOCHROMAT, NA = 1.46). For determining the FA area, fluorescence images were imported into MATLAB (Mathworks), and regions of interest (ROI) were manually drawn around individual cells. Using a custom-written MATLAB program, the FA signal was extracted by convoluting the image (Gaussian structure element; width, 25; height, 2) and applying a top-hat filtering step (disk, SE; radius, 7 pixels) as described before[43]. For FA analysis, the area of each FA mask was used to calculate the mean FA size per cell.

Ratiometric Förster resonance energy transfer. Ratiometric FRET analysis of living cells was performed on a Leica SP8 confocal laser scanning microscope equipped with a 63× water objective (HCX PL APO, NA = 1.2); cells were excited at 514 nm, and intensities of donor (522–550 nm) and acceptor (600–700 nm) emission were recorded simultaneously. To isolate FA-specific signals, the MATLAB program described above was employed. As before, the FA signal was extracted by convoluting the image and applying a top-hat filtering step; the resulting FA masks were used

© 2017 Nature America, Inc., part of Springer Nature. All rights reserved.

to calculate a mean FA intensity of donor and acceptor signal. Ratiometric FRET values were then calculated by mean intensity acceptor/donor division as described[9].

ROCK inhibitor (Y-27632) experiments. Cells were allowed to spread on FN-coated glass coverslips O/N. For FLIM analysis, Y-27632 (final concentration, 1 μM) was added to the medium, and lifetime images were recorded after 12 min of incubation. Effects of ROCK inhibition were analyzed by acquiring an initial FRET ratio image, then adding Y-27632 (1 μM) and acquiring FRET ratio images after 6 min and 12 min. The FA signal was extracted, using the MATLAB algorithm described above, followed by a two-class Otsu thresholding, which was necessary to extract the comparably weak FA signal that is characteristic for ROCK-inhibited cells. The mean acceptor values were only used if they were 1.3 times larger than the manually determined average background signal.

Fluorescence recovery after photobleaching. For the characterization of turnover rates of talin-YPet and talin-FL-1973, we performed FRAP experiments with cells seeded on Y-shaped FN-coated micropatterned substrates (CYTOO)[9]. Briefly, using a Leica SP8 confocal laser scanning microscope equipped with a 63× water objective (HCX PL APO, NA = 1.2) cells were excited at 514 nm with a laser power of 5% to record two prebleach images every 10 s. After photobleaching of a selected FA with 100% laser power for 1 s, postbleach images were acquired every 20 s for a period of 280 s. The fluorescence emission was recorded between 530–570 nm. For data analysis, the ImageJ plugin 'FRAP profiler' was used to extract raw fluorescence recovery curves, which were then normalized to the minimal and maximal intensity using MATLAB. The mean as well as the s.e.m. of the normalized data was calculated and plotted against time after photobleaching. To determine the fluorescence recovery, we fitted the data assuming a reaction-dominated model as described[44] using data with a fitting quality of $R^2 \geq 0.98$. Mobile fraction (A) and half-time of recovery ($\tau_{1/2}$) values were extracted and plotted individually.

Time-correlated single-photon-counting fluorescence lifetime microscopy. Live-cell TCSPC-FLIM experiments were performed on a confocal laser scanning microscope (Leica TCS SP5 X). The instrument was equipped with a pulsed white light laser (WLL, 80 MHz repetition rate; NKT Photonics), a FLIM X16 TCSPC detector (LaVision Biotech), and a 63× water objective (HCX PL APO CS, NA = 1.2); a bandpass filter 545/30 (AHF Analysentechnik; Chroma) was used to block photons emitted by the acceptor fluorophore. Images were acquired with a scanning velocity of 400 Hz, a spatial resolution of 512 × 512 pixels, and resulting image field coverage of 123.02 × 123.02 μm^2. For each experimental condition, 15–20 cells were recorded, and this procedure was repeated on 2–5 individual days. Custom-written MATLAB programs based on previously published software[9] were used for the subsequent data analysis. As illustrated in **Supplementary Figure 5**, an ROI was manually drawn around the cell of interest, and the FA signal was extracted by multi-Otsu thresholding with three intensity classes. Next, a histogram of photon arrival times of the donor fluorophore was fitted by a monoexponential decay function, and if the fit quality was sufficiently high ($R^2 > 0.98$) the data were used to calculate the fluorescence lifetime of the donor in the absence or presence of the acceptor fluorophore. FRET efficiency E was calculated according to equation (14), where τ_D is the mean donor only lifetime, and τ_{DA} is the lifetime of the donor in presence of an acceptor fluorophore.

$$E = 1 - \frac{\tau_{DA}}{\tau_D} \quad (14)$$

Thus, the described procedure provides the average FRET efficiency of all FAs from one individual cell; this value is displayed as one data point in the respective box plots. As the experiments typically used more than 30 cells, the data are based upon a couple of hundred to thousands of individual FAs.

Live-cell fluorescence lifetime imaging microscopy. To determine live-cell FRET efficiencies of talin constructs, live-cell dishes (81158; ibidi) were coated with either FN (10 μg/ml) or poly-L-Lysine (pLL, 0.1% (w/v)). For FN experiments, cells were seeded O/N; for the pLL control, cells were seeded for 5 min. To investigate the dependence of talin tension on substrate stiffness, cells were seeded on softview dishes (coated with 10 μg/ml FN), and fluorescence lifetime measurements were performed using a 40× long-distance water objective (APO 40× /1.10W CORR C S2). Intermolecular FRET was determined by fluorescence lifetime measurements in Tln1$^{-/-}$/Tln2$^{-/-}$ cells coexpressing either talin-YPet-447 and talin-mCherry-447 or talin-YPet-1973 and talin-mCherry-1973. Fluorescence lifetime measurements of mCherry-tagged constructs were performed using an excitation wavelength of 586 nm.

Single excitation wavelength dual-color TCSPC-FLIM. Live-cell dual-color TCSPC-FLIM experiments were performed using a Leica SP8 confocal laser scanning microscope equipped with a 440 nm pulsed diode laser (40 MHz repetition rate), a 63× immersion oil objective (HCPL APO CS2, NA = 1.4) and the PicoHarp 300 TCSPC module (PicoQuant). Cells were seeded on FN-coated Lab-Tek Chamber Slides (ThermoFisher Scientific) and allowed to spread O/N. Images of living cells were acquired with a laser intensity of 10 μW, a scanning velocity of 400 Hz, a spatial resolution of 512 × 512 pixels, and a resulting image field coverage of 92.26 × 92.26 μm^2 per channel; the emitted fluorescence was split into two channels at 467–499 nm and 525–565 nm. Photons in the first channel were detected by a single-photon-counting detector module (PDM; Micro Photon Devices); photons in the second channel were detected by a red-sensitive single-photon avalanche diode (TauSPAD; PicoQuant). For data analysis, the SymphoTime software (PicoQuant) was employed; an ROI was set for each cell manually, and the fluorescence lifetime values in each channel were determined by fitting a monoexponential decay curve to the respective histogram of photon arrival times. FRET efficiencies were calculated according to equation (14).

Algorithm to calculate molecular stretch ratio. To estimate the amount of mechanically engaged sensor molecules from TCSPC-FLIM data, we assumed that the observed histogram of photon arrival times comprises two underlying fluorescence lifetimes: the fluorescence lifetime of FL-TSM in the closed (c) and in the stretched (s) state, which correspond to the folded and unfolded conformation of the FL peptide. Under this assumption, the

© 2017 Nature America, Inc., part of Springer Nature. All rights reserved.

doi:10.1038/nmeth.4431

experimentally determined fluorescence lifetime decays can be described by a biexponential function

$$P(t) = A_s e^{-\frac{t}{\tau_s}} + A_c e^{-\frac{t}{\tau_c}} + P_{bg} \quad (15)$$

where A_s and A_c are initial photon count rates from stretched molecules with lifetime τ_s and closed molecules with lifetime τ_c; P_{bg} is the background photon count rate. We note that, for long observation times, the photon count for molecules in the stretched and non-stretched state $N_{s,c}$ is approximated by

$$N_{s,c} \approx \int_0^\infty A_{s,c} e^{-\frac{t}{\tau_{s,c}}} dt = A_{s,c}\tau_{s,c} \quad (16)$$

where the indices reference to either stretched (s) or closed (c) states. Thus, equation (15) can be rewritten as

$$P(t) = \frac{N_s}{\tau_s} e^{-\frac{t}{\tau_s}} + \frac{N_c}{\tau_c} e^{-\frac{t}{\tau_c}} + P_{bg} \quad (17)$$

Under the assumption that the total sensor photon count N is the sum of photons from the stretched N_s and closed N_c sensor molecules, the relative amount of photons in the stretched state r_N is defined by

$$r_N = \frac{N_s}{N} \quad (18)$$

and equation (17) can be rewritten as

$$P(t) = N\left(\frac{r_N}{\tau_s} e^{-\frac{t}{\tau_s}} + \frac{1-r_N}{\tau_c} e^{-\frac{t}{\tau_c}}\right) + P_{bg} \quad (19)$$

As FRET reduces the amount of photons emitted by the donor fluorophore, the relative amount of photons r_N is not equivalent to the relative amount of molecules r_M. Here, we use the approximation that the number of molecules $M_{s,c}$ is proportional to the number of photons and inversely related to the fluorescence lifetime[45]

$$M_{s,c} \propto \frac{N_{s,c}}{\tau_{s,c}} \quad (20)$$

which allows reformulation of equation (19). The molecular stretch ratio is then described by equation (21), as shown in **Figure 6b**.

$$r_M = \frac{M_s}{M} = \frac{r_N\tau_c}{r_N\tau_c + (1-r_N)\tau_s} \quad (21)$$

Thus, equation (19) can be rewritten as

$$P(t) = \frac{N}{r_M\tau_s + (1-r_M)\tau_c}\left(r_M e^{-\frac{t}{\tau_s}} + (1-r_M)e^{-\frac{t}{\tau_c}}\right) + P_{bg} = P_M\left(r_M e^{-\frac{t}{\tau_s}} + (1-r_M)e^{-\frac{t}{\tau_c}}\right) + P_{bg} \quad (22)$$

Calculation of molecular stretch ratio. The biexponential model in equation (15) has five free parameters, two of which can be experimentally determined to increase the fit robustness. The lifetime of the non-stretched, closed FL-TSM (τ_c) can be extracted from control experiments in which FL-TSM is C terminally attached to the protein of interest. Given the large contour length increase of FL-TSM under force, the fluorescence lifetime of the stretched sensor (τ_s) is equal to the lifetime of YPet, which can also be measured (**Fig. 6a**).

Data fits were performed using the maximum likelihood function $L_{poisson}$ to account for the underlying statistics of TCSPC-FLIM measurements. The photon counts in each time bin i of the width Δt are Poisson distributed, and the assumption that their mean value $n_i \approx\sim P(t_i)\Delta t$ is a good approximation when Δt is considerably shorter than the fluorescence lifetimes ($\Delta t << \tau_{s,c}$) Thus, we used equation (23):

$$L_{Poisson}(n;m) = \prod_i \frac{e^{-n_i} n_i^{m_i}}{m_i!}, \quad (23)$$

where m_i is the experimentally measured photon count per time bin. The application of the maximum likelihood function as a point estimator was performed by solving the negative logarithm of equation (23) with the built-in MATLAB function 'FMINSEARCH'. To determine the relative amount of photons emitted from stretched molecules $r_N \in [0,1]$, boundaries for r_N were implemented by using the transformation $r_N = (1 - \sin\rho)/2$ and fitting ρ[46].

Estimation of the minimally required photon number. To a priori estimate the lower bound for the total number of photons N_t required for the determination of stretch ratio r_M, we assume that the experimental data are described by the biexponential model. The probability p_i that a photon is detected in bin i is then given by

$$p_i = (1-b)\left[r_M \frac{\left(e^{\frac{\Delta t}{\tau_s}} - 1\right)e^{-\frac{t_i}{\tau_s}}}{1 - e^{-\frac{t_i}{\tau_s}}} + (1-r_M)\frac{\left(e^{\frac{\Delta t}{\tau_c}} - 1\right)e^{-\frac{t_i}{\tau_c}}}{1 - e^{-\frac{t_i}{\tau_c}}}\right] + \frac{b}{N_t} \quad (24)$$

where b is the relative amount of background photons, Δt the bin width, and $\tau_{s,c}$ the lifetimes of stretched or closed sensor. Assuming that the Cramér–Rao inequality for unbiased estimators holds, the variance σ^2 is bounded by

$$\sigma_{pg}{}^2 \geq \frac{I_{pq}^{-1}}{N_t},$$

where

$$I_{pq} = \sum_i \frac{1}{p_i}\left(\frac{dp_i}{dx_p}\right)\left(\frac{dp_i}{dx_q}\right)$$

In this way, the minimum number of photons can be calculated for a given target variance σ^{*2}. Based on these calculations, photon count histograms were used if at least 10,000 photons were collected. Note that in these cases, the raw data for fitting monoexponential or biexponential models were identical.

Statistical analysis. Error bars indicate the s.e.m. if not indicated otherwise. Bar plots display the mean value and the s.d. as error bars. Normal distribution of FRAP data was confirmed by the Lillifors test. For statistical evaluation of FLIM data, a two-sided

© 2017 Nature America, Inc., part of Springer Nature. All rights reserved.

Kolmogorov–Smirnov test with a default significance level of $\alpha = 0.05$ (two-sided) was used; the thereby calculated statistical significance was given by a P value. Additional testing was performed with a paired t-test (significance level of $\alpha = 0.05$, two-sided) and the two-sided Mann–Whitney U test ($\alpha = 0.05$), as indicated. The following nomenclature was used in all figures: ***, $P < 0.001$; **, $P < 0.01$; *, $P < 0.05$; not significant, n.s., $P > 0.05$. Box plots were generated using the MATLAB function 'boxplot()', indicating the median (indicated by red line), the 25th and the 75th percentiles, as well as whiskers that reach out to 1.5 interquartile range (IQR) corresponding to 2.7 s.d. (σ) for normally distributed data. Detailed information on the statistics of each data set can be found in **Supplementary Table 1**; and additional background information on sample size and data exclusion is provided in the **Life Sciences Reporting Summary**.

Computational codes. Mechanical fits for the force spectroscopy analysis were performed using previously published custom-written code[42]; the analysis software code runs on IGOR Pro 6.31, 64-bit. Software for FA-FRAP and TCSPC-FLIM analyses was published before[9] and can be used in MATLAB. Computational codes are available upon request.

Data availability statement. The authors confirm that all relevant data are included in this published article (and its supplementary information files). Additional data that support the findings of this study are available upon request. Accession codes: HP35-TSM (MF685010), F40-TSM (MF685012) and FL-TSM (MF685013).

37. Austen, K., Kluger, C., Freikamp, A., Chrostek-Grashoff, A. & Grashoff, C. Generation and analysis of biosensors to measure mechanical forces within cells. *Methods Mol. Biol.* **1066**, 169–184 (2013).
38. von Hansen, Y., Mehlich, A., Pelz, B., Rief, M. & Netz, R.R. Auto- and cross-power spectral analysis of dual trap optical tweezer experiments using Bayesian inference. *Rev. Sci. Instrum.* **83**, 095116 (2012).
39. Tolić-Nørrelykke, S.F. *et al.* Calibration of optical tweezers with positional detection in the back focal plane. *Rev. Sci. Instrum.* **77**, 103101 (2006).
40. Moffitt, J.R., Chemla, Y.R., Izhaky, D. & Bustamante, C. Differential detection of dual traps improves the spatial resolution of optical tweezers. *Proc. Natl. Acad. Sci. USA* **103**, 9006–9011 (2006).
41. Wang, M.D., Yin, H., Landick, R., Gelles, J. & Block, S.M. Stretching DNA with optical tweezers. *Biophys. J.* **72**, 1335–1346 (1997).
42. Stigler, J., Ziegler, F., Gieseke, A., Gebhardt, J.C. & Rief, M. The complex folding network of single calmodulin molecules. *Science* **334**, 512–516 (2011).
43. Würflinger, T., Gamper, I., Aach, T. & Sechi, A.S. Automated segmentation and tracking for large-scale analysis of focal adhesion dynamics. *J. Microsc.* **241**, 37–53 (2011).
44. Sprague, B.L. & McNally, J.G. FRAP analysis of binding: proper and fitting. *Trends Cell Biol.* **15**, 84–91 (2005).
45. Verveer, P.J., Squire, A. & Bastiaens, P.I. Global analysis of fluorescence lifetime imaging microscopy data. *Biophys. J.* **78**, 2127–2137 (2000).
46. James, F. *Statistical Methods in Experimental Physics* 2nd edn. (World Scientific Publishing Co., 2006).

© 2017 Nature America, Inc., part of Springer Nature. All rights reserved.

doi:10.1038/nmeth.4431

nature research

Corresponding author(s): Carsten Grashoff

☐ Initial submission ☐ Revised version ☒ Final submission

Life Sciences Reporting Summary

Nature Research wishes to improve the reproducibility of the work that we publish. This form is intended for publication with all accepted life science papers and provides structure for consistency and transparency in reporting. Every life science submission will use this form; some list items might not apply to an individual manuscript, but all fields must be completed for clarity.

For further information on the points included in this form, see Reporting Life Sciences Research. For further information on Nature Research policies, including our data availability policy, see Authors & Referees and the Editorial Policy Checklist.

Experimental design

1. Sample size

Describe how sample size was determined.

For FLIM data analysis, we performed statistical tests with simulated data to ensure that a sample size of 3 experiments with each 10-20 cells is sufficient to draw conclusions about significance. Variation of data was compared to values generated from Poisson statistics (information not shown in the manuscript).

2. Data exclusions

Describe any data exclusions.

As far as possible, data analysis procedures were standardized by custom written MATLAB programs. All data of the same type was evaluated using identical software settings and programs.
- for FRAP analysis only cells with sufficient photo-bleaching (< 20% of initial value) and within a pre-defined intensity range were admitted and only recovery curves with a mono-exponential fit yielding R-square > 0.98 were included (see online Methods)
- for data from TCSPC-FLIM experiments, only lifetimes from cells with sufficient fit quality (R>0.98) were taken into consideration, as described (ref.9).
- for dual-color TCSPC-FLIM, only cells with maximal photon count per pixel higher than 100 was used .
- for biexponential fitting, only data with a minimal photon count of 10000 and an $\chi 2$ of ≥0.1 was considered.

3. Replication

Describe whether the experimental findings were reliably reproduced.

All experiments were performed at independent experimental days and showed similar tendencies. Fluorescence lifetime imaging microscopy data was independently reproduced using ratiometric FRET analysis.

4. Randomization

Describe how samples/organisms/participants were allocated into experimental groups.

-

5. Blinding

Describe whether the investigators were blinded to group allocation during data collection and/or analysis.

-

Note: all studies involving animals and/or human research participants must disclose whether blinding and randomization were used.

© 2017 Nature America, Inc., part of Springer Nature. All rights reserved.

Nature Methods: doi:10.1038/nmeth.4431

6. Statistical parameters

For all figures and tables that use statistical methods, confirm that the following items are present in relevant figure legends (or in the Methods section if additional space is needed).

n/a	Confirmed
☐	☒ The exact sample size (*n*) for each experimental group/condition, given as a discrete number and unit of measurement (animals, litters, cultures, etc.)
☐	☒ A description of how samples were collected, noting whether measurements were taken from distinct samples or whether the same sample was measured repeatedly
☐	☒ A statement indicating how many times each experiment was replicated
☐	☒ The statistical test(s) used and whether they are one- or two-sided (note: only common tests should be described solely by name; more complex techniques should be described in the Methods section)
☐	☒ A description of any assumptions or corrections, such as an adjustment for multiple comparisons
☐	☒ The test results (e.g. *P* values) given as exact values whenever possible and with confidence intervals noted
☐	☒ A clear description of statistics including central tendency (e.g. median, mean) and variation (e.g. standard deviation, interquartile range)
☐	☒ Clearly defined error bars

See the web collection on statistics for biologists for further resources and guidance.

Software

Policy information about availability of computer code

7. Software

Describe the software used to analyze the data in this study.

-FRET(force)-Model established as described in online Methods, the analysis software code runs on: IGOR Pro 6.31, 64-bit.
-Matlab R2016b, custom-written programms for FRAP analysis, mono-and bi-exponential lifetime fitting.
-Code for FRAP analysis and mono-exponential fitting is based on the analysis that was published previously (ref. 9).
-Bi-exponential lifetime fitting is described in detail in the online Methods.
-Mean FA size Analysis code is based on previously published Focal Adhesion Tracking algorithm (ref.43).
-For mulitplexing of FRET sensors, the SymPhoTime64 software from Picoquant was used.

For manuscripts utilizing custom algorithms or software that are central to the paper but not yet described in the published literature, software must be made available to editors and reviewers upon request. We strongly encourage code deposition in a community repository (e.g. GitHub). *Nature Methods* guidance for providing algorithms and software for publication provides further information on this topic.

Materials and reagents

Policy information about availability of materials

8. Materials availability

Indicate whether there are restrictions on availability of unique materials or if these materials are only available for distribution by a for-profit company.

The generated DNA plasmids will be made available through addgene (http://www.addgene.org/). All suppliers that distribute materials for profit are indicated in the online Methods section.
To obtain talin 1/2 double knockout cells, please contact Reinhard Faessler (MPI of Biochemistry).

9. Antibodies

Describe the antibodies used and how they were validated for use in the system under study (i.e. assay and species).

anti-vinculin (hVIN-1) (V9131, Sigma; IF 1:200), anti-paxillin (610051, BD Transduction L.; IF 1:400), anti-p-MLC (Ser19) (3671, NEB; IF 1:50), anti-mouse IgG–Alexa Fluor-405 (A31553; IF 1:400; Thermo Fisher Scientific), Alexa Fluor-647 phalloidin (A22287; IF 1:200; Thermo Fisher Scientific) (Methods p.10)

© 2017 Nature America, Inc., part of Springer Nature. All rights reserved.

Nature Methods: doi:10.1038/nmeth.4431

10. Eukaryotic cell lines

a. State the source of each eukaryotic cell line used.

- talin 1/2 double knockout cells: fibroblastoid kidney cells of a three week-old mouse
-vinculin knockout cells: mouse embryonic fibroblast cell line

b. Describe the method of cell line authentication used.

No authentication

c. Report whether the cell lines were tested for mycoplasma contamination.

Parental cell lines were tested for contamination. Results were negative.

d. If any of the cell lines used are listed in the database of commonly misidentified cell lines maintained by ICLAC, provide a scientific rationale for their use.

No commonly misidentified cell lines were used.

Animals and human research participants

Policy information about studies involving animals; when reporting animal research, follow the ARRIVE guidelines

11. Description of research animals

Provide details on animals and/or animal-derived materials used in the study.

None

Policy information about studies involving human research participants

12. Description of human research participants

Describe the covariate-relevant population characteristics of the human research participants.

None

© 2017 Nature America, Inc., part of Springer Nature. All rights reserved.

Nature Methods: doi:10.1038/nmeth.4431